Somato-Dendritic Morphology Predicts Physiology for Neurons That Contribute to Several Kinds of Limb Movements

Ari Berkowitz, Gina L. C. Yosten and R. Mark Ballard

JN 95:2821-2831, 2006. First published Feb 1, 2006; doi:10.1152/jn.01246.2005

Journal of Neurophysiology publishes original articles on the function of the nervous system. It is published 12 times a year (monthly) by the American Physiological Society, 9650 Rockville Pike, Bethesda MD 20814-3991. ISSN: 0022-3077, ESSN: 1522-1598. Visit our website at http://www.the-aps.org/.

J Neurophysiol 95: 2821–2831, 2006.
First published February 1, 2006; doi:10.1152/jn.01246.2005.

Somato-Dendritic Morphology Predicts Physiology for Neurons That Contribute to Several Kinds of Limb Movements

Ari Berkowitz, Gina L. C. Yosten, and R. Mark Ballard
Department of Zoology, University of Oklahoma, Norman, Oklahoma

Submitted 29 November 2005; accepted in final form 25 January 2006

Berkowitz, Ari, Gina L. C. Yosten, and R. Mark Ballard. Somato-dendritic morphology predicts physiology for neurons that contribute to several kinds of limb movements. *J Neurophysiol* 95: 2821–2831, 2006. First published February 1, 2006; doi:10.1152/jn.01246.2005. It has been difficult to predict the behavioral roles of vertebrate CNS neurons based solely on their morphologies, especially for the neurons that control limb movements in adults. We examined the morphologies of spinal interneurons involved in limb movement control, using intracellular recording followed by Neurobiotin injection in the in vivo adult turtle spinal cord preparation. We report here the first description of a class of spinal interneurons whose somato-dendritic morphologies predict their robust activity during multiple forms of ipsilateral and contralateral fictive hindlimb scratching and fictive hindlimb withdrawal. These "transverse interneurons" or T cells have a mediolaterally elongated soma and a simple dendritic tree that is extensive in the transverse plane but restricted rostrocaudally. During fictive scratching, these cells display strong rhythmic modulation with higher peak firing rates than other scratch-activated interneurons. These higher peak firing rates are at least partly caused by T cells having larger phase-locked membrane potential oscillations and narrower action potentials with briefer afterhyperpolarizations than other scratch-activated interneurons. Many T cells have axon terminal arborizations in the ventral horn of the spinal cord hindlimb enlargement. Identification of this morphological and physiological class of spinal interneurons should facilitate further exploration of the mechanisms of hindlimb motor pattern selection and generation.

INTRODUCTION

A neuron's morphology often provides clues to its physiological role in a circuit. In many small, invertebrate nervous systems, individual neurons can be repeatedly identified from one animal to the next, facilitating exploration of each cell's structure and function (Marder and Calabrese 1996). In vertebrates, individually identifiable neurons are rare, but identification of correlated morphological and physiological properties of cells has been valuable in elucidating the operational mechanisms of neuronal circuits.

This approach has been successful, for example, in deciphering how the lamprey (Buchanan 2001; Grillner 2003) and embryonic tadpole (Li et al. 2001; Roberts 2000) spinal cords generate axial swimming movements. It has been quite difficult, however, to find morphological parameters that predict the physiological activity or behavioral role of adult mammalian spinal cord neurons, probably because of the greater complexity of adult mammalian nervous systems. For example, adult cat spinal neurons have been extensively studied with respect to their differential inputs from classes of sensory neurons and several brain areas, but each neuron typically receives convergent inputs from multiple sources and the roles of neurons in limb movement control cannot be reliably distinguished on morphological grounds alone (Edgley 2001; Jankowska 1992).

The search for morphological indicators of function in limb movement control is likely to be more feasible in spinal cords that are smaller and simpler than those of adult mammals. Thus one fruitful approach is to study animals early in development (Clarac et al. 2004; Kiehn and Butt 2003; O'Donovan et al. 1998). A second approach is to study adult, nonmammalian spinal cords that generate complex limb movements using fewer neurons, and perhaps fewer types of neurons, than adult mammalian spinal cords (Cheng et al. 2002; Stein 2005).

We searched for morphological predictors of limb movement function using the adult turtle spinal cord, which can appropriately produce the motor patterns underlying three forms of hindlimb scratching, forward swimming, and withdrawal (flexion reflex), even without input from the brain and movement-related sensory feedback (Stein 2005). Scratching and withdrawal can be elicited by naturalistic mechanical stimulation of the shell or skin, in the absence of artificial pharmacological or electrical stimulation. Moreover, turtles are unusually resistant to hypoxia, which facilitates physiological study for longer periods than are possible in analogous mammalian preparations (Hounsgaard and Nicholson 1990; Lutz et al. 2003).

Much has been learned about the spinal control of scratching, swimming, and withdrawal from in vivo turtle studies (Stein 2005) and about the morphology and physiology of spinal neurons from in vitro turtle studies (Fernandez et al. 1996; Gorman et al. 2005; Hounsgaard and Kjaerulff 1992; McDonagh et al. 1998, 2002; Russo and Hounsgaard 1996a,b; Stauffer et al. 2005). Only recently, however, has intracellular recording of turtle spinal interneurons been applied in vivo, facilitating examination of the morphology and physiology of individual interneurons that contribute to limb movements (Berkowitz 2005). We describe here a new class of turtle spinal interneurons whose morphology predicts its robust activity during multiple forms of scratching bilaterally and during limb withdrawal.

METHODS

Animal preparation

In anesthetized adult red-eared turtles (*Trachemys scripta elegans*, 500–1,200 g, $n = 29$), the spinal cord was transected between the

Address for reprint requests and other correspondence: A. Berkowitz, Dept. of Zoology, Univ. of Oklahoma, 730 Van Vleet Oval, Norman, OK 73019 (E-mail: ari@ou.edu).

The costs of publication of this article were defrayed in part by the payment of page charges. The article must therefore be hereby marked "*advertisement*" in accordance with 18 U.S.C. Section 1734 solely to indicate this fact.

dorsal 2 (D2) and D3 dorsal roots, the spinal cord was exposed from the D6 through the sacral 2 (S2) segments, and several hindlimb motor nerves were exposed and dissected free, including the right and left hip flexor motor nerves and several right knee extensor motor nerves (Berkowitz 2001a; Robertson et al. 1985). The animal was immobilized with gallamine (8 mg/kg) and artificially respirated at room temperature. All animal procedures were approved by the Institutional Animal Care and Use Committee of the University of Oklahoma.

Electrophysiology

Electroneurograms (ENGs) were obtained from hindlimb motor nerves using pairs of 100-μm silver wire in mineral oil, amplified (1,000 times), and band-pass-filtered (0.1–1 kHz). Intracellular recordings were obtained from the gray matter on the right side of the hindlimb enlargement (D_8, D_9, D_{10}, S_1, and S_2 segments) spinal cord, using sharp microelectrodes made from thin-walled borosilicate glass with a filament (Sutter Instrument Co., Novato, CA), fabricated with a P-97 puller (Sutter) and filled with 4% Neurobiotin (Vector Laboratories, Burlingame, CA) dissolved in 1 M KCl, with resistances of 60–120 MΩ. The intracellular electrode was advanced using a piezoelectric microdrive (Inchworm, Burleigh Instruments, Fishers, NY), and impalements were often facilitated using 5-ms negative capacitance "tickle" pulses delivered by the intracellular amplifier (World Precision Instruments, Sarasota, FL). A small amount of constant hyperpolarizing current was sometimes used to maintain the membrane potential at about –70 mV. Fictive hindlimb scratching or withdrawal was elicited by gentle mechanical stimulation of one site at a time, using a glass probe with a fire-polished tip attached to a force transducer (Grass-Telefactor, West Warwick, RI). All signals were stored using a digital audio tape recorder (TEAC America, Montebello, CA) and analyzed off-line using Datapac 2000 software (Run Technologies, Laguna Hills, CA).

Neurobiotin injection and histology

After physiological characterization of a cell, sinusoidal (4 Hz) current with a peak depolarization of +0.1–3.0 nA was injected for 1–30 min to eject Neurobiotin. No more than one interneuron fill was attempted in each spinal cord segment, to ensure unambiguous identification. After the last cell fill, the animal was anesthetized with pentobarbital and transcardially perfused with saline and 4% chilled paraformaldehyde. The D8-S2 spinal cord was postfixed overnight at 4°C, cryoprotected in 20% sucrose, embedded in a gelatin-albumin-glutaraldehyde medium, and frozen-sectioned at 100 μm horizontally. Sections were rinsed, incubated 30 min in 0.3% H_2O_2, rinsed, incubated overnight at 4°C in 1:100 ABC solution (Vector)/0.3% Triton X-100, rinsed, reacted 4–7 min in 0.5 times Vector SG solution, and rinsed again (Berkowitz 2005). Sections were mounted, air-dried, counterstained in Fast Nuclear Red (Vector), dehydrated in graded ethanols, cleared, and mounted.

Morphological analysis

Intereurons ($n = 47$) were included in this study only if *1*) they were activated or rhythmically modulated during fictive scratching, *2*) one and only one stained soma with attached stained processes was recovered at the expected site, and *3*) for ventral horn neurons, the processes were darkly stained and yet no stained process was seen in a ventral root; motoneurons (Fig. 3) additionally had a single stained axon within a ventral root. Reconstructions were made through a camera lucida from the serial horizontal sections; digital photomicrographs were obtained with a DP-70 camera (Olympus America, Melville NY). Rostrocaudal and mediolateral dendritic extent and number of dendritic branch points were measured from reconstructions of all 47 interneurons. Dorsoventral dendritic extent was estimated from the number of horizontal sections containing portions of the dendrites. For dendritic lengths, we focused on measurements of ratios rather than absolute values to exclude effects caused by possible variability in the completeness of staining. Soma mean diameter was calculated as the average of the major and minor axis diameters in horizontal sections. Rostrocaudal and mediolateral soma length were measured from high-magnification camera lucida tracings of the somata alone.

Physiological analysis

The modulation of each interneuron's firing rate was quantitatively analyzed separately during each form of ipsilateral fictive scratching in which *1*) there were clear, alternating bursts and silent intervals of the ipsilateral hip flexor motor nerve, *2*) at least two such cycles of fictive scratching occurred, and *3*) the interneuron fired at least 10 action potentials during these cycles. In each such case, a dual-referent phase histogram (with 5 bins for the hip flexor burst and 5 bins for the hip flexor interburst interval) was calculated with respect to the rectified and smoothed bursts and interburst intervals of the ipsilateral hip flexor nerve, using Datapac 2000 (Berkowitz 2001b, 2002; Berkowitz and Stein 1994a). The phase histogram data were used to calculate the mean vector (Batschelet 1981; Berkowitz and Stein 1994a; Drew and Doucet 1991; Mardia 1972). The mean vector length (MVL) is a measure of the degree of rhythmic modulation of a neuron's activity with respect to a cycle; it can vary from 0 to 1, with 0 indicating minimal rhythmicity and 1 indicating maximal rhythmicity. The null hypothesis that the interneuron's firing occurred at random with respect to the hip flexor cycle was evaluated using the Rayleigh test (Batschelet 1981; Berkowitz and Stein 1994a; Drew and Doucet 1991; Mardia 1972). The mean vector angle is a measure of the phase preference of a neuron with the hip flexor cycle; it can vary from 0 to 1 (or 0–360°), with 0 to 0.5 (or 0–180°) indicating a phase preference during hip flexor activity, and 0.5 to 1 (or 180–360°) indicating a phase preference within the hip flexor interburst intervals. Mean vector angles were used in analyses only if the phase histogram passed the Rayleigh test with $P < 0.01$ (Berkowitz 2001b, 2002; Berkowitz and Stein 1994a).

Most cells were active during multiple forms of fictive scratching, so multiple phase histograms were constructed for each cell, each including all acceptable cycles of scratching obtained at that site of stimulation; the phase histogram used for each cell's MVL was the one that passed the Rayleigh test with the lowest P value, unless multiple phase histograms had $P < 0.001$, in which case the one among these having the highest MVL was used (Berkowitz 2001b, 2002; Berkowitz and Stein 1994a). The cell's peak firing rate during ipsilateral fictive scratching was taken as the highest mean firing rate out of the 10 bins of a cell's phase histogram. For one type of analysis (Fig. 5*A*), the phase histogram used was the one that passed the Rayleigh test with the lowest probability of the null hypothesis (or, when multiple phase histograms had $P < 0.01$, the 1 among those with the highest MVL); for a second type of analysis (Fig. 5*B*), the phase histogram used was the one that included the cell's highest mean firing rate during 1 of its 10 bins. Action potential widths, afterhyperpolarization (AHP) peak amplitudes, and AHP durations (from the start of the AHP till decay to half-maximal AHP amplitude) were measured from averages of 10–20 consecutive action potentials that occurred while the interneuron was firing at a low rate, using Datapac 2000.

To calculate dual-referent phase-averaged membrane potential oscillations, action potentials were deleted from the intracellular recording (and the missing voltage values interpolated from the values just before and after the action potential), the recording was then linearly smoothed with a time constant of 200 ms, and the signal was dual-referent phase-normalized and averaged for all cycles of fictive scratching at that site of stimulation, using Datapac 2000. The phase-averaged oscillation used in further analysis for each cell was from the site used for its MVL, unless the cell fired <10 action potentials for

each site of ipsilateral scratching, in which case the ipsilateral site with the largest phase-averaged oscillation was used.

RESULTS

We recorded from and recovered the morphology of 47 scratch-activated interneurons with somata in the hindlimb enlargement of the spinal cord. These neurons were studied in vivo while mechanically eliciting multiple forms of fictive scratching and hindlimb withdrawal bilaterally. The physiology, axon trajectories, and axon-terminal arborizations of these cells, taken as a single group, have already been reported (Berkowitz 2005). We describe here that a subset of these cells, defined by their somato-dendritic features, seems to form a morphological and physiological class that is likely to play an important role in limb movement control. We call these cells "transverse interneurons" or T cells.

T cells are strongly and rhythmically activated during scratching

T cells were strongly activated during multiple forms of fictive scratching of both the ipsilateral and the contralateral hindlimb and usually were activated during ipsilateral hindlimb withdrawal as well. For example, the T cell shown in Fig. 1 was rhythmically activated during ipsilateral rostral (Fig. 1*A*), pocket (Fig. 1*B*), and caudal fictive scratching (Fig. 1*C*), as well as contralateral pocket (Fig. 1*E*) and caudal fictive scratching (Fig. 1*F*). In addition, this cell was activated during ipsilateral fictive hindlimb withdrawal (Fig. 1*G*), received rhythmic subthreshold depolarizations during contralateral rostral scratching (Fig. 1*D*), and was depolarized during contralateral hindlimb withdrawal (Fig. 1*H*). It displayed strong rhythmic modulation of firing that was phase-locked to the scratch rhythm and its peak firing rate during scratching was unusually high for turtle spinal neurons (Fig. 1, *A–F*). The high degree of rhythmic modulation and high rate of peak firing during scratching were correlated with large, phase-locked oscillations of the membrane potential.

Morphologically, T cells were unusually simple (e.g., Fig. 1*I*). The soma typically was in the intermediate zone or ventral horn and was small and mediolaterally elongated. The primary dendrites emerged from the medial and lateral ends of the soma and their orientation was almost entirely within the transverse plane. The dendritic tree was smooth, with few or no spines and was extensively elongated dorsoventrally and mediolaterally, often approaching the pial surface laterally, but was relatively restricted rostrocaudally. There were only a small number of secondary dendrites and few higher-order dendrites. The axon, when it could be seen, emerged from the soma with a ventral trajectory and traveled either exclusively within the gray matter or also within the white matter immediately adjacent to the gray matter.

We quantitatively analyzed the physiology of all the interneurons during ipsilateral fictive scratching by separately assessing each cell's firing rate and membrane potential oscillations. We analyze firing rates using dual-referent phase histograms of the interneuron's mean firing rate with respect to the ipsilateral hip flexor motor nerve's activity cycle; phase values of 0–0.5 are during the hip flexor burst, while values of 0.5–1 are during the interburst interval. The MVL for each phase histogram indicates

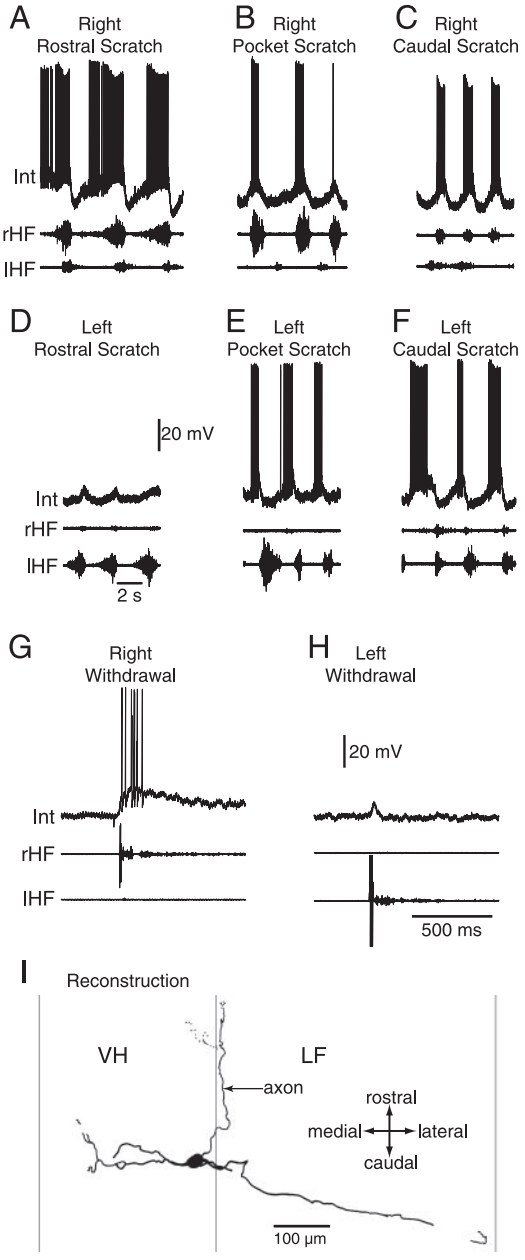

FIG. 1. Example of a transverse interneuron (T cell). *A–H*: each set of traces shows a recording of the same T cell (Int), whose soma was in the dorsal part of the ventral horn of the right D8 segment, along with the right (rHF) and left (lHF) hip flexor motor nerves, during fictive scratching (*A–F*) or fictive hindlimb withdrawal (*G* and *H*). Note that the cell was strongly activated with a high degree of rhythmic modulation during multiple forms of scratching, bilaterally, and was also activated during ipsilateral limb withdrawal. *I*: reconstruction of this T cell. Note the mediolaterally elongated soma, the dendrites extending laterally to the edge of the lateral funiculus (LF), and the axon terminal arborization in the ventral horn (VH).

to what extent the interneuron's action potentials were concentrated within the hip flexor cycle; a value of 0 would indicate a random distribution with respect to the cycle, whereas a value of 1 would indicate that all action potentials occurred within 10% of the cycle. We analyzed membrane potential oscillations using dual-referent phase-normalized averages of the membrane potential with respect to the ipsilateral hip flexor cycle during ipsilateral fictive scratching, after deleting the action potentials and then smoothing the signals.

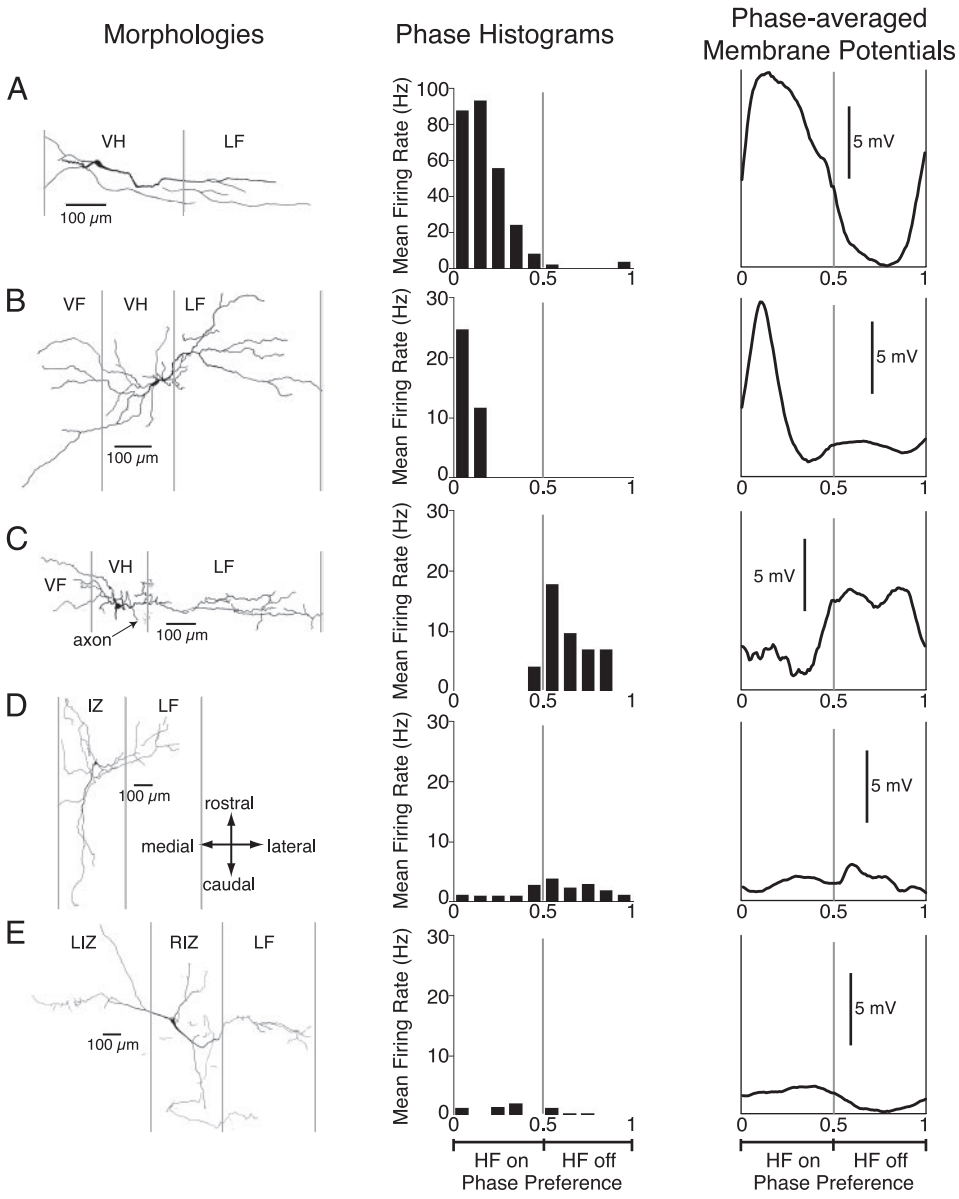

FIG. 2. Morphologies, phase histograms, and phase-averaged membrane potentials of example T cells and non-T cells. *A–C*: morphologies (*left*), dual-referent phase histograms of firing rates with respect to the ipsilateral HF motor nerve during ipsilateral fictive scratching (*middle*), and dual-referent phase-averaged membrane potentials during ipsilateral fictive scratching (*right*) for 3 T cells. *D* and *E*: morphologies (*left*), phase histograms (*middle*), and phase-averaged membrane potentials (*right*) for 2 cells with very different morphologies (non-T cells). Note that T cells seem to fire at higher rates, have greater rhythmic modulation, and have larger membrane potential oscillations than non-T cells. IZ, intermediate zone; LF, lateral funiculus; LIZ, left intermediate zone; RIZ, right intermediate zone; VF, ventral funiculus; VH, ventral horn.

The phase histograms showed that T cells typically had high peak firing rates during fictive scratching and had their action potentials concentrated within a particular phase of the scratch cycle, with different T cells having different phase preferences (Fig. 2, *A–C*, *middle*). The phase-averaged membrane potentials showed that T cells typically had large membrane potential oscillations that peaked in a particular phase of the scratch cycle, which corresponded to their phase of peak firing (Fig. 2, *A–C*, *right*). Other scratch-activated spinal interneurons (non-T cells) had diverse morphologies that differed from T cells; most saliently, their dendritic trees had a more rostrocaudal orientation (Fig. 2, *D* and *E*, *left*). Non-T cells typically had lower firing rates and weaker rhythmic modulation during fictive scratching than T cells (Fig. 2, *D* and *E*, *middle*), as well as smaller phase-locked membrane potential oscillations (Fig. 2, *D* and *E*, *right*). Spinal motoneurons recorded in this study, like T cells, had large membrane potential oscillations during ipsilateral fictive scratching, but tended to have higher action potential thresholds and lower firing rates during fictive scratching than T cells (Fig. 3; see also Alaburda et al. 2005; Robertson and Stein 1988).

T cells, defined by quantitative somato-dendritic parameters, have higher peak firing rates

Thus subjectively defined T cells and non-T cells differed in their morphologies, peak firing rates, degrees of rhythmic modulation, and amplitudes of phase-locked membrane potential oscillations. We wondered if a subset of the morphological parameters that distinguish T cells from other scratch-activated interneurons could be used quantitatively to predict differences in the physiological activity of these cells. We recognized that there probably is continuous (rather than discrete) variation in both the morphological and the physiological parameters of scratch-activated spinal interneurons. We reasoned that the probability of finding morphological parameters that predict physiological differences would be increased if we compared groups of neurons at opposite ends of a morphological spec-

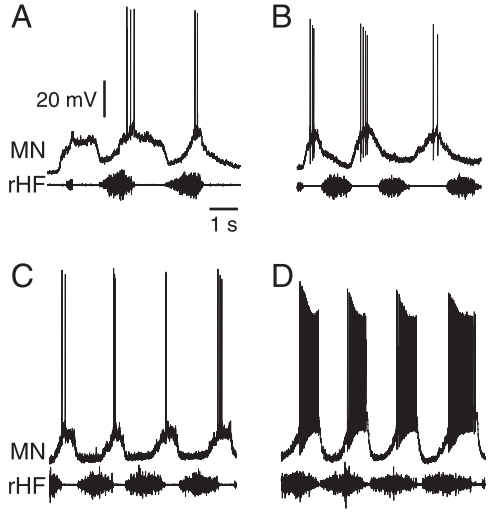

FIG. 3. Hindlimb motoneuron behavior during ipsilateral fictive scratching. *A–D*: examples of intracellularly recorded hindlimb motoneurons (MN) during ipsilateral fictive scratching, along with the ipsilateral rHF, for comparison with interneurons. Somata of these motoneurons were in the D9 (*A*), S2 (*B*), D10 (*C*), and S1 (*D*) segments.

trum. Some of the most salient morphological features of T cells are a dendritic tree that is extensive mediolaterally (M-L) and dorsoventrally (D-V) but relatively restricted rostrocaudally (R-C) and a soma that is mediolaterally elongated. Thus we measured the length of the dendritic tree along each axis and the length of the soma rostrocaudally and mediolaterally. We operationally defined T cells as cells having a dendritic length ratio, R-C/(M-L + D-V), of <0.4 and a soma length ratio, R-C/M-L, of ≤ 1.0 (Fig. 4*A*). This rule defined a group of 17 cells that was clustered within the "space" of somato-dendritic length ratios (Fig. 4*A*) and had somata in the deepest dorsal horn, the intermediate zone, and the dorsal half of the ventral horn (Fig. 4*B*).

Within this group of 17 T cells, only 5 (29%) were spontaneously active (although this number might not be reliable because of 2 factors: the impalement itself, which would tend to depolarize the cell, and a small amount of constant hyperpolarizing current that was sometimes applied to stabilize the recording). Of the 17 T cells, 16 (94%) were active during all three forms of ipsilateral fictive scratching (the remaining cell was activated during 1 form). In addition, 13 (76%) of these cells were activated during all three forms of contralateral fictive scratching (3 others were activated during 2 of the 3 forms and the remaining cell during 1 form), 15 (88%) were activated during ipsilateral fictive withdrawal (the remaining 2 were each hyperpolarized), and during contralateral fictive withdrawal 2 were activated, 2 received subthreshold depolarization, and 1 was hyperpolarized. The activity with respect to the ipsilateral hip flexor cycle during fictive scratching was sufficiently rhythmic to pass the Rayleigh test (with $P < 0.01$) for 14 (82%) of these 17 cells during at least one form of ipsilateral scratching. These cells had phase preferences (mean vector angles) within the ipsilateral hip flexor cycle that tended to be the same during all three forms of ipsilateral scratching (rostral vs. pocket: $r = 0.77$, $n = 8$; $P = 0.01$; rostral vs. caudal: $r = 0.92$, $n = 6$, $P = 0.005$; pocket vs. caudal: $r = 0.85$, $n = 9$, $P = 0.003$), as has been seen previously for scratch-activated interneurons generally (Berkowitz 2001b, 2005; Berkowitz and Stein 1994a).

We operationally defined a comparison group of non-T cells at the opposite end of a morphological spectrum, as those scratch-activated interneurons with a dendritic length ratio, R-C/(M-L + D-V), of >0.5 (Fig. 4*A*), which we think captures the most salient distinction between T cells and scratch-activated cells with quite different morphologies. This rule defined a morphologically heterogeneous group of 14 cells (Fig. 4*A*) with somata in the dorsal horn, the intermediate zone, and the dorsal half of the ventral horn, similar to the locations of the T cell somata (Fig. 4*B*). The mean soma diameters of T cells tended to be somewhat less than those of non-T cells, but this apparent difference was not statistically significant (T cells mean ± SE: 18.9 ± 1.1 μm; non-T cells: 20.5 ± 1.2 μm; $P = 0.15$, Mann-Whitney *U* test). Likewise, T cells tended to have fewer dendritic branches than non-T cells, but this apparent difference was not quite statistically significant (T cells mean ± SE: 15.9 ± 3.8; non-T cells: 21.1 ± 3.4; $P = 0.08$, Mann-Whitney *U* test); this measure, however, may be especially sensitive to the completeness of staining.

We then assessed whether there were consistent physiological differences between the group of T cells and the group of non-T cells that were defined by these quantitative somato-dendritic parameters. The T cells had an average peak firing rate during fictive scratching that was about three times as high as that of the non-T cells (Fig. 5). This was true for the peak firing rates during the form of ipsilateral scratching in which the cell was most rhythmic (i.e., had the highest MVL; T cells:

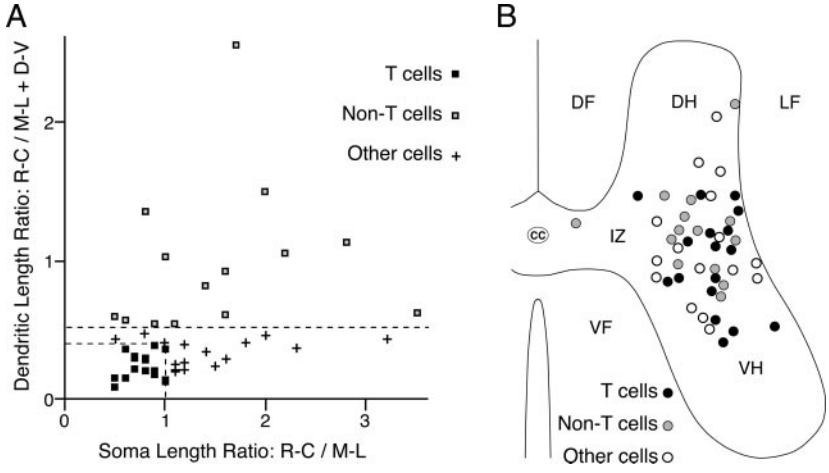

FIG. 4. Quantitative morphological classification of T cells and non-T cells. *A*: plot of dendritic length ratios, rostrocaudal (R-C) dendritic length/[mediolateral (M-L) dendritic length + dorsoventral (D-V) dendritic length] vs. soma length ratios, R-C/M-L, for all scratch-activated interneurons. Cells with a dendritic length ratio of <0.4 and a soma length ratio of ≤ 1.0 were operationally classified as T cells (black squares). Cells with a dendritic length ratio of >0.5 were classified as non-T cells (gray squares). *B*: soma locations of T cells (black circles), non-T cells (gray circles), and other scratch-activated interneurons (white circles) shown on a schematic cross-section with respect to the borders of the dorsal horn (DH), IZ, and VH. CC, central canal; DF, dorsal funiculus; LF, lateral funiculus; VF, ventral funiculus.

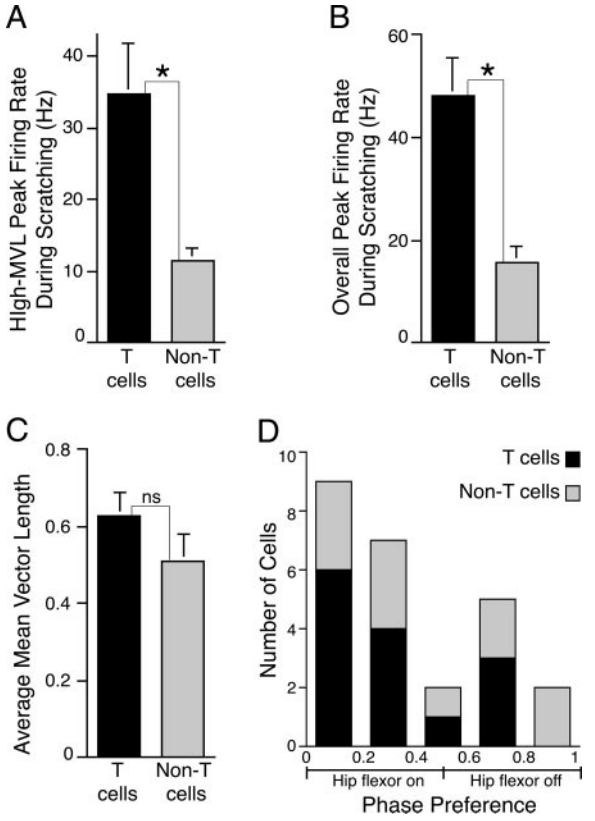

FIG. 5. Firing rate modulation of T cells and non-T cells. *A*: mean peak firing rates ± SE for T cells ($n = 15$) and non-T cells ($n = 14$) during the form of ipsilateral fictive scratching that passed the Rayleigh test with the lowest probability of the null hypothesis, or, if multiple forms had $P < 0.01$, for the one among them that had the highest mean vector length (MVL, a measure of the degree of rhythmic modulation). *B*: mean peak firing rates ± SE for T cells ($n = 15$) and non-T cells ($n = 14$) during the form of ipsilateral fictive scratching with the highest interneuron peak firing rate. *C*: average MVLs ± SE for T cells ($n = 15$) and non-T cells ($n = 14$). *D*: histogram of phase preferences (mean vector angles) within the ipsilateral hip flexor cycle during ipsilateral fictive scratching for T cells ($n = 14$) and non-T cells ($n = 11$). *$P < 0.05$, Mann-Whitney *U* test; NS, not significant.

34.9 ± 6.9 Hz; non-T cells: 11.4 ± 1.9 Hz; $P = 0.001$, Mann-Whitney *U* test; Fig. 5*A*), as well as for the highest peak firing rates during any form of ipsilateral scratching (T cells: 48.1 ± 7.5 Hz; non-T cells: 15.8 ± 3.1 Hz; $P = 0.0003$, Mann-Whitney *U* test; Fig. 5*B*). The firing rates of the T cells also showed somewhat greater rhythmic modulation during fictive scratching (i.e., they had a higher average MVL) than non-T cells did, although this apparent difference was not statistically significant (T cells average MVL: 0.63 ± 0.06; non-T cells: 0.51 ± 0.07; $P = 0.13$, Mann-Whitney *U* test; Fig. 5*C*). The preferred phases of firing for both T cells and non-T cells were distributed across the hip flexor cycle, although no T cells were encountered with a preferred phase at the very end of the hip flexor interburst interval (Fig. 5*D*).

T cells have narrower spikes, briefer afterhyperpolarizations, and larger oscillations

The higher peak firing rates that T cells displayed during fictive scratching could be the result of at least two nonmutually exclusive mechanisms. One possible mechanism is that the action potentials of T cells are briefer than those of non-T cells and/or involve shorter refractory periods, allowing the spikes to occur in more rapid succession. We measured the spike widths, the AHP amplitudes, and the AHP durations (from the start of the AHP till the half-maximal AHP amplitude) for all cells (Fig. 6*A*). For the sample of interneurons taken as a whole, spike widths, and AHP durations were each negatively correlated with overall peak firing rates, although these correlations were not quite statistically significant (peak firing rates vs. spike widths: $r = -0.24$; $n = 41$, $P = 0.07$; peak firing rates vs. AHP duration: $r = -0.23$; $n = 41$, $P = 0.07$). Nonetheless, there were large and statistically significant differences between the T cell group and the non-T cell group in average spike width and average AHP duration. The average spike width of the non-T cells was 52% greater than that of the T cells (T cells: 2.08 ± 0.26 ms; non-T cells: 3.16 ± 0.53 ms; $P = 0.03$, Mann-Whitney *U* test; Fig. 6*B*). The average AHP amplitudes of the T cells and the non-T cells were similar (T cells: 8.05 ± 1.16 mV; non-T cells: 7.80 ± 1.62 mV; $P = 0.30$, Mann-Whitney *U* test; Fig. 6*C*), but the average AHP duration of the non-T cells was about three times as long as that of the T cells (T cells: 3.95 ± 0.72 ms; non-T cells: 12.82 ± 2.95 ms; $P = 0.03$, Mann-Whitney *U* test; Fig. 6*D*).

A second possible mechanism is that T cells receive larger rhythmic depolarizations than non-T cells, which help drive them to higher peak firing rates. We assessed this second possibility using the scratch phase-normalized averages of interneurons' membrane potential oscillations for all T cells and all non-T cells. We measured the amplitude of the average oscillation for each cell, as well as the peak and trough phases (Fig. 7*A*). For both T cells and non-T cells, peak phases (and trough phases) differed considerably among neurons, with the trough phase typically occurring about half a cycle after the peak phase (Fig. 7*B*). The mean amplitude of the oscillations, however, was about 69% greater in T cells than non-T cells (T cells: 6.96 ± 0.77 mV; non-T cells: 4.11 ± 0.49 mV; $P = 0.007$, Mann-Whitney *U* test; Fig. 7*C*).

Other cells

Morphological and physiological parameters for the group of "other cells" were variable, but often intermediate between T cells and non-T cells. On average, the soma diameters of other cells (21.0 ± 1.4 μm) were significantly greater than those of T cells ($P = 0.04$; Mann-Whitney *U* test) and similar to those of non-T cells ($P = 0.25$). The number of dendritic branches of other cells (12.9 ± 1.9) was similar to that of T cells ($P = 0.44$) and probably less than that of non-T cells ($P = 0.051$). Other cells were quite rhythmic during scratching (MVL: 0.70 ± 0.07), similar to T cells ($P = 0.29$), and significantly more rhythmic than non-T cells ($P = 0.04$). Other cells had peak firing rates during scratching (highest MVL rate: 20.4 ± 2.7 Hz; overall highest rate: 30.8 ± 7.0 Hz) that were less than those of T cells ($P = 0.08$ and $P = 0.02$, respectively) and significantly more than those of non-T cells ($P = 0.02$ and $P = 0.02$, respectively). Other cells had narrow action potentials (1.56 ± 0.13 ms), similar to those of T cells ($P = 0.08$), but significantly less than those of non-T cells ($P = 0.001$). The AHP amplitudes of other cells (10.8 ± 1.1 mV) were significantly greater than those of T cells ($P = 0.04$) and perhaps also non-T cells ($P = 0.06$). The AHP durations of other cells (13.1 ± 3.5 ms) were significantly greater than

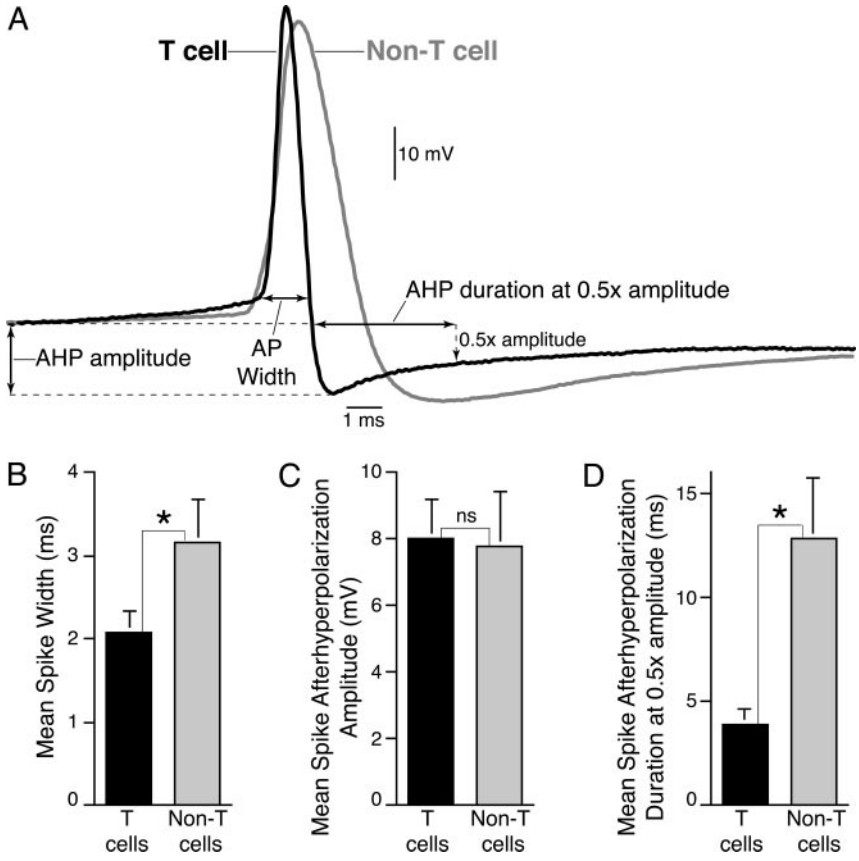

FIG. 6. Action potential characteristics of T cells and non-T cells. *A*: averaged action potentials (APs) of a representative T cell (black) and a representative non-T cell (gray), along with an illustration of the AP parameters measured (shown for the T cell): AP width, afterhyperpolarization (AHP) peak amplitude, and AHP duration (from the start of the AHP till decay to the half-maximal amplitude). *B*: mean spike width ± SE for T cells (n = 17) and non-T cells (n = 14). *C*: mean spike AHP peak amplitude ± SE for T cells (n = 17) and non-T cells (n = 14). *D*: mean spike AHP duration to half-maximal amplitude ± SE for T cells (n = 17) and non-T cells (n = 14). *$P < 0.05$, Mann-Whitney U test; NS, not significant.

those of T cells ($P = 0.002$) and similar to those of non-T cells ($P = 0.39$). Finally, the amplitudes of scratch oscillations in other cells (6.4 ± 1.3 mV) were intermediate between T cells and non-T cells but not significantly different from either (vs. T cells: $P = 0.16$; vs. non-T cells: $P = 0.24$).

We also assessed whether the T-cell morphological criterion based on the ratio of dendritic extent [(R-C/M-L + D-V) < 0.4] alone would be sufficient to predict physiological differences between T cells and non-T cells, in the absence of the soma ratio criterion (R-C/M-L ≤ 1.0). T cells defined by this single criterion had significantly fewer dendritic branches (14.7 ± 3.0) than non-T cells ($P = 0.04$) and still had significantly higher peak firing rates (highest MVL rate: 29.1 ± 5.2 Hz; overall highest rate: 42.6 ± 6.5 Hz) than non-T cells ($P = 0.004$ and $P = 0.001$, respectively), as well as significantly narrower action potentials (1.97 ± 0.17 ms) than non-T cells ($P = 0.01$). However, their AHP durations (6.79 ± 1.29 ms) and their scratch oscillation amplitudes (6.03 ± 0.62 mV) were not significantly different from non-T cells ($P = 0.13$ and $P = 0.06$, respectively), in contrast to the two-criteria definition of T cells. The soma diameter (19.2 ± 0.96 μm), MVL (0.64 ± 0.04), and AHP amplitude (9.31 ± 0.96 mV) were also (as before) not significantly different from those of non-T cells ($P = 0.31$, $P = 0.07$, and $P = 0.15$, respectively). Thus the ratio of dendritic extent is by itself a good predictor of several physiological parameters, but the ratio of soma lengths also contributes to predicting some physiological parameters.

T cells can have ventral horn axon terminals

The strong activation and strong rhythmic modulation of T cells during fictive scratching suggests that T cells play important roles in production of limb motor output. To have any direct effect on limb motor output, T cells should have synaptic outputs within the hindlimb enlargement region of the spinal cord, probably within the ventral horn, if not in the ventrolateral ventral horn, where the somata of limb motoneurons are. Thus we examined the axon trajectories and axon terminal arborizations of the T cells, which would give a strong indication of the locations of at least some of the T cell output synapses.

As a group, the T cells had very narrow parent axons (≪1 μm), at the limits of what can be seen clearly under the light microscope and apparently even thinner than those of other scratch-activated spinal interneurons (Berkowitz 2005). Perhaps for this reason, staining of T cell axons was patchy, as has been noted in general for axons stained intracellularly with biotinylated compounds or horseradish peroxidase (McDonagh et al. 2002). Nonetheless, axons could be followed for some distance for 11 of the 17 T cells. The axon trajectories of T cells were diverse, although all visible axons either remained in the gray matter or traveled in the white matter immediately adjacent to the gray matter. The axons of three cells traveled in the ipsilateral lateral funiculus (1 ascended, 1 descended, and 1 bifurcated) and those of three others traveled in the ipsilateral ventral funiculus (1 ascended, 1 descended, and 1 bifurcated; the cell with the descending axon also had an axon collateral that crossed and bifurcated within the contralateral gray matter). The axons of five other T cells crossed the spinal cord and traveled in the contralateral ventral funiculus (1 ascended, 2 descended, and 2 bifurcated).

Axon trajectories could also be followed for 8 of the 14 non-T cells. One descended in the ipsilateral lateral funiculus,

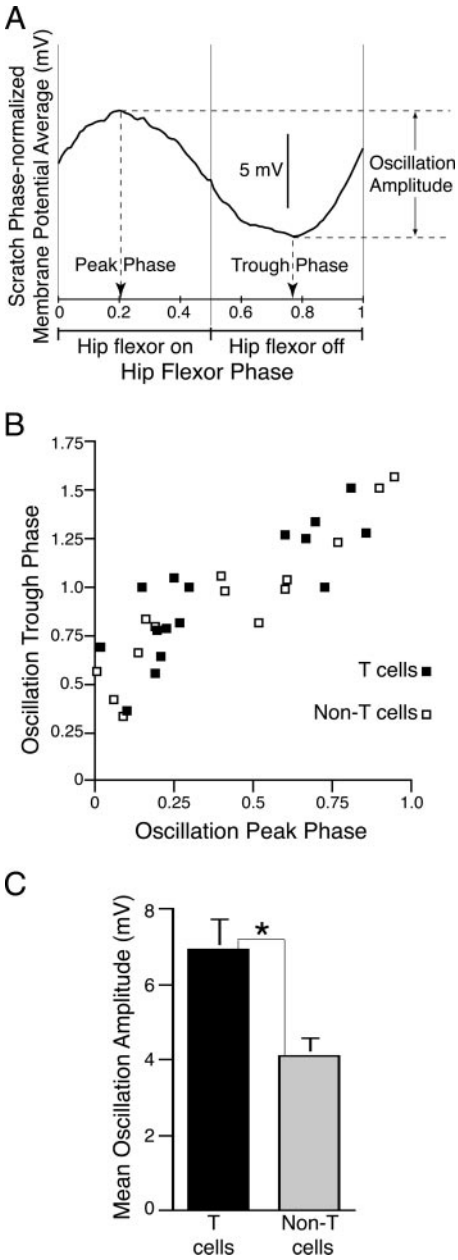

FIG. 7. Phase-averaged membrane potential oscillations of T cells and non-T cells. *A*: example of a dual-referent hip flexor phase-normalized membrane potential oscillation during ipsilateral fictive scratching, along with a schematic illustration of the measurement of the peak phase, the trough phase, and the oscillation amplitude. *B*: relationship between peak phase and trough phase for all T cells and non-T cells. *C*: mean oscillation amplitude ± SE for T cells ($n = 16$) and non-T cells ($n = 14$).

two traveled in the ipsilateral ventral funiculus (1 descended and 1 bifurcated), two remained within the ipsilateral gray matter (1 ascended and 1 bifurcated), and three crossed and traveled in the contralateral ventral funiculus (1 ascended, 1 descended, and 1 bifurcated; the cell with the ascending axon also had an axon that bifurcated within the ipsilateral gray matter).

Figure 8 shows the reconstruction and representative photomicrographs of one T cell that had numerous axon terminal arborizations within the ipsilateral ventral horn, including the ventrolateral ventral horn. These terminal arborizations included characteristic dark spherical or ovoid swellings attached to extremely thin axon terminal branches. Axon terminal arborizations could be seen for 12 of the 17 T cells. The axon terminals of 9 of these 12 cells were found exclusively in the ipsilateral ventral horn; another had axon terminals in the ipsilateral dorsal horn and intermediate zone and the remaining 2 cells had axon terminals in the contralateral ventral horn.

Eight of the 14 non-T cells also had identifiable axon terminals. Three were in the ipsilateral ventral horn alone, one was in the ipsilateral dorsal horn alone, two were in the ipsilateral intermediate zone and ventral horn, one was in the ipsilateral dorsal horn, intermediate zone, and ventral horn, and one was in the contralateral ventral horn.

DISCUSSION

We have described here a new morphological and physiological class of spinal interneurons involved in limb movement control, which we call transverse interneurons or T cells. T cells are rhythmically activated during multiple forms of fictive scratching bilaterally and often are activated during limb withdrawal as well. Their dendritic trees extend far into the white matter mediolaterally, but are relatively short rostrocaudally and have relatively few higher-order branches. T cells have unusually high peak firing rates during fictive scratching, due at least partly to their having larger phase-locked membrane

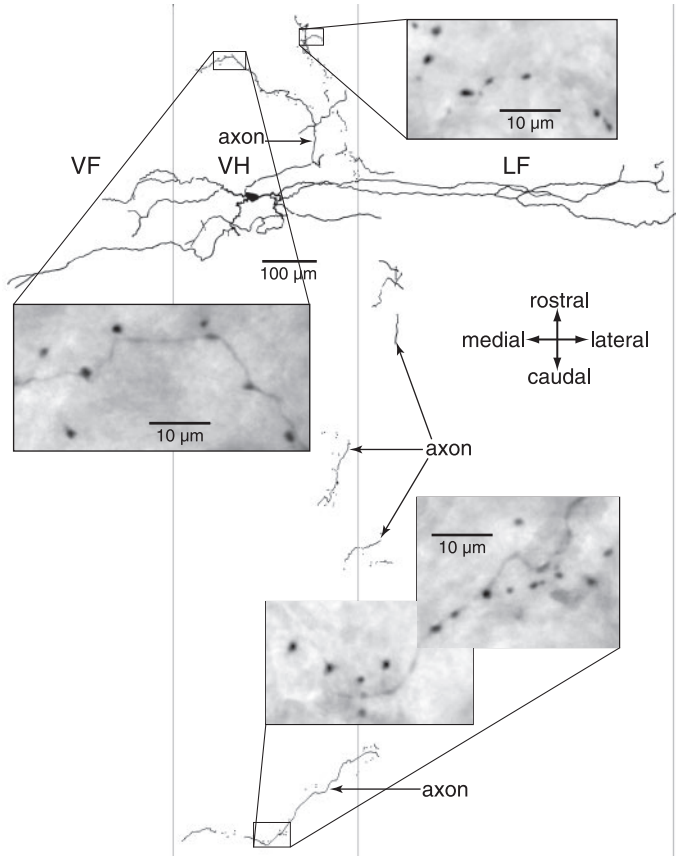

FIG. 8. Axon terminal arborizations of a T cell. Reconstruction of a T cell and high-magnification photomicrographs (*insets*), showing axon terminal arborizations in the ipsilateral ventral horn, including some in the ventrolateral ventral horn, where hindlimb motoneuron somata are located. LF, lateral funiculus; VF, ventral funiculus; VH, ventral horn.

TABLE 1. *Summary of Differences Between T cells and Non-T cells*

	Dendritic Extent	Peak Firing Rate During Scratching	Action Potential Width	AHP Duration	Scratch Oscillation Amplitude
T cells	Longer mediolaterally and dorsoventrally	Higher	Shorter	Shorter	Larger
Non-T cells	Longer rostrocaudally	Lower	Longer	Longer	Smaller

AHP, after hyperpolarization.

potential oscillations and narrower action potentials with briefer afterhyperpolarizations than other scratch-activated interneurons (Table 1). Many T cells have axon terminal arborizations in the ventral horn. This set of physiological and morphological characteristics suggests that T cells play important roles in limb movement control.

Several features of T cells raise the possibility that they are last-order premotor interneurons. First, the strong rhythmic modulation and high peak firing rates of T cells should allow them to elicit the large membrane potential oscillations and robust rhythms seen in motoneurons during fictive scratching (Fig. 3; see also Alaburda et al. 2005; Robertson and Stein 1988). Motoneurons, having unusually large somata and unusually complex dendritic trees (McDonagh et al. 1998, 2002; Ruigrok et al. 1984), may require either simultaneous inputs from a large number of premotor interneurons or inputs from rhythmic premotor interneurons that have especially high peak firing rates, as T cells do. Second, T cells, having dendrites that extend far into the lateral funiculus and ventral funiculus, are positioned to receive and integrate inputs from a wide variety of ascending and descending propriospinal and descending brain sources that are known to modulate hindlimb motor patterns (Drew et al. 2004; Grillner and Dubuc 1988; Orlovsky et al. 1999) and may make en passant synapses within the white matter (Berkowitz and Stein 1994b). Third, T cells have small somata that are easily driven beyond action potential threshold, which may allow their inputs to be especially effective in driving them. Thus T cells may transform relatively weak rhythmic inputs from other scratch-activated interneurons into the large phase-locked membrane potential oscillations that may be required of premotor interneurons. Fourth, many T cells have axon terminal arborizations in the ventral horn, including the ventrolateral ventral horn, where limb motoneuron somata are located (Ruigrok and Crowe 1984). Given the diversity of their phase preferences and axon terminations, different T cells may activate or inhibit different hindlimb motor pools, including both ipsilateral and contralateral motor pools. Given their strong rhythmicity during fictive scratching, T cells might also contribute to scratch motor pattern generation.

Our morphological and physiological data on T cells facilitate comparisons with turtle spinal interneurons studied in vivo and in vitro. The strongly rhythmic activity of T cells during multiple forms of scratching bilaterally and activity typically during withdrawal as well is consistent with their being a subset of "scratch/swim neurons," which are activated during scratching, forward swimming, and often additional hindlimb motor patterns (Berkowitz 2002); however, tests of this prediction will have to await a further set of experiments in a preparation that also produces swimming motor patterns. T cell somata are distributed similarly to those of descending propriospinal neurons (Berkowitz and Stein 1994b). The strongly rhythmic activity of T cells and their predominantly ventral soma locations may partly account for the previously observed correlation between depth and rhythmicity of scratch-activated spinal interneurons (Berkowitz 2001b).

T cell somato-dendritic morphologies are virtually identical to one hindlimb enlargement intermediate zone cell from a juvenile turtle (*Emys europaea*) displayed in Banchi's Golgi-stained material (Fig. 12 in Banchi 1903). The small ventral horn somata and extensive transverse plane dendrites of T cells appear consistent with either or both populations of turtle ventral horn interneurons, one having plateau potentials and one not, studied in slice preparations (Hounsgaard and Kjaerulff 1992), but inconsistent with plateau-generating (Russo and Hounsgaard 1996b) and burst-generating (Russo and Hounsgaard 1996a) dorsal horn neurons and giant neurons (Fernandez et al. 1996). The T cell somato-dendritic orientations, simple dendritic trees, and brief spike afterhyperpolarizations appear more similar to nonspontaneously active than spontaneously active turtle ventral horn interneurons studied in slice preparations (McDonagh et al. 1998, 2002); most T cells also did not have spontaneous activity under our conditions. Mean soma diameters of T cells were smaller than six turtle ventral horn interneurons from slice preparations studied in detail (McDonagh et al. 2002). High-threshold ventral horn interneurons in slice preparations displayed higher mean firing rates and shorter mean afterhyperpolarizations than low-threshold interneurons (Stauffer et al. 2005), similar to two distinctions between T cells and non-T cells.

The spinal cord is largely conserved (Fetcho 1992; Kusuma et al. 1979; Nieuwenhuys 1964), so interneurons homologous to T cells may occur in other vertebrates. Many adult lamprey spinal neurons have dendritic trees that are extensive mediolaterally but short rostrocaudally; this appears especially true of contralateral, caudal interneurons, and excitatory interneurons (Buchanan 2001). The T cell somato-dendritic morphology is not obviously similar to spinal interneurons described in embryonic zebrafish (Bernhardt et al. 1990; Hale et al. 2001), *Xenopus* (Li et al. 2001), or chick (Yaginuma et al. 1994), but these embryonic neurons have relatively limited dendritic trees, making comparisons to adult neurons difficult.

In mammals, Golgi staining has shown that many intermediate zone and ventral horn neurons have dendritic trees that are extensive in the transverse plane but restricted rostrocaudally (Brown 1981; Scheibel and Scheibel 1969); most, however, appear much more extensive dorsoventrally than mediolaterally, whereas T cells dendrites are consistently extensive mediolaterally; thus cells homologous to T cells may be a subset of this group. T cells have similar soma locations and somato-dendritic morphologies to ipsilaterally projecting horizontal cells and some lateral cells (Silos-Santiago and Snider 1994), as well as several types of commissural cells (intero-medial-lateral border cells, horizontal cells in the intermediate

zone, and oblique cells in the intermediate zone and ventral horn) (Silos-Santiago and Snider 1992) in embryonic rats. Adult cat midlumbar neurons receiving input from group II muscle afferents have lamina VII somata and dendrites that are longer mediolaterally and dorsoventrally than rostrocaudally (Bras et al. 1989), like T cells. Adult cat inhibitory interneurons receiving input from group Ia muscle afferents also have lamina VII somata, but their dendritic trees are least extensive mediolaterally (Rastad et al. 1990), unlike T cells. Adult cat Renshaw cells have somata in the ventralmost ventral horn and short, radial dendrites (Bui et al. 2003; Fyffe 1990), unlike T cells. Some adult cat lamina VI-VIII commissural neurons that receive reticulospinal input, are rhythmically active during fictive locomotion, and have ventral horn axon terminals do have somato-dendritic morphologies similar to T cells (Matsuyama et al. 2004); some also fire with strong rhythmic modulation and high peak firing rates during fictive locomotion (e.g., their Fig. 9).

Morphological distinctions among spinal interneurons have often emphasized soma locations and axon projections and terminations (Bernhardt et al. 1990; Hale et al. 2001; Jankowska 1992; Li et al. 2001; Nissen et al. 2005; Oppenheim et al. 1988; Roberts 2000; Yaginuma et al. 1994); this seems appropriate given that axon terminations indicate probable synaptic targets. This approach to morphological categorization has also identified spinal neurons that have particular soma locations in early development (Bernhardt et al. 1990; Hale et al. 2001; Nissen et al. 2005; Yaginuma et al. 1994) and that play particular roles in axial movement control (Buchanan 2001; Grillner 2003; Higashijima et al. 2004; Li et al. 2001; Roberts 2000). Axon projections have also matched up to some degree with subpopulations born at particular times and expressing particular early transcription factors, facilitating selective labeling and deletion (Butt et al. 2005; Caspary and Anderson 2003; Higashijima et al. 2004; Hinckley et al. 2005; Lanuza et al. 2004; Lewis 2006; Li et al. 2004; Wilson et al. 2005). These experiments hold great promise for elucidating limb movement control circuits, although it appears unlikely that a subpopulation expressing any one transcription factor has a single axon projection pattern or plays a single role in adult limb movement control (Butt et al. 2005; Higashijima et al. 2004; Lewis 2006; Li et al. 2004; Nissen et al. 2005; Sharma and Peng 2001; but see also Hinckley et al. 2005; Wilson et al. 2005).

In addition to soma locations, axon projections, and transcription factor expression in development, somato-dendritic morphologies can also help guide functionally relevant categorical distinctions and have been useful in many studies (Bernhardt et al. 1990; Buchanan 2001; Bui et al. 2003; Hale et al. 2001; Matsuyama et al. 2004; Scheibel and Scheibel 1969; Silos-Santiago and Snider 1992, 1994). Moreover, several categories of spinal interneurons based partly on axon projections are actually variable with respect to whether the axon ascends, descends, or bifurcates (Bernhardt et al. 1990; Hale et al. 2001; Li et al. 2001; Oppenheim et al. 1988), suggesting that distinctions in axon direction may not be necessary or sufficient to establish functionally relevant categories. Extensive and distinct dendritic architectures may also be a more prominent feature of spinal interneurons in adult, limbed vertebrates than those in adult limbless vertebrates or in embryonic vertebrates. We hope that this study encourages interest in somato-dendritic parameters as a subset of the tools that may be brought to bear to uncover functionally relevant populations of spinal interneurons contributing to limb movements.

ACKNOWLEDGMENTS

We thank Dr. Joseph Bastian for numerous helpful discussions and Drs. Bastian and Paul S. G. Stein for comments on a previous version of this manuscript.

GRANTS

This work was supported by National Science Foundation Grants 9807991 and 0349620 to A. Berkowitz and an accompanying Research Experiences for Undergraduates Supplement for G.L.C. Yosten.

REFERENCES

Alaburda A, Russo R, MacAulay N, and Hounsgaard J. Periodic high-conductance states in spinal neurons during scratch-like network activity in adult turtles. *J Neurosci* 25: 6316–6321, 2005.

Banchi A. La minuta struttura della midolla spinale dei Chelonii (*Emys europaea*). *Arch Ital Anat Embriol* 2: 291–307 and Tav. XXVIII–XXXI, 1903.

Batschelet E. *Circular Statistics in Biology* London: Academic Press, 1981.

Berkowitz A. Broadly tuned spinal neurons for each form of fictive scratching in spinal turtles. *J Neurophysiol* 86: 1017–1025, 2001a.

Berkowitz A. Rhythmicity of spinal neurons activated during each form of fictive scratching in spinal turtles. *J Neurophysiol* 86: 1026–1036, 2001b.

Berkowitz A. Both shared and specialized spinal circuitry for scratching and swimming in turtles. *J Comp Physiol [A]* 188: 225–234, 2002.

Berkowitz A. Physiology and morphology indicate that individual spinal interneurons contribute to diverse limb movements. *J Neurophysiol* 94: 4455–4470, 2005.

Berkowitz A and Stein PSG. Activity of descending propriospinal axons in the turtle hindlimb enlargement during two forms of fictive scratching: phase analyses. *J Neurosci* 14: 5105–5119, 1994a.

Berkowitz A and Stein PSG. Descending propriospinal axons in the turtle hindlimb enlargement: cells of origin and funicular courses. *J Comp Neurol* 346: 321–336, 1994b.

Bernhardt RR, Chitnis AB, Lindamer L, and Kuwada JY. Identification of spinal neurons in the embryonic and larval zebrafish. *J Comp Neurol* 302: 603–616, 1990.

Bras H, Cavallari P, Jankowska E, and Kubin L. Morphology of midlumbar interneurones relaying information from group II muscle afferents in the cat spinal cord. *J Comp Neurol* 290: 1–15, 1989.

Brown AG. *Organization in the Spinal Cord.* Berlin: Springer-Verlag, 1981.

Buchanan JT. Contributions of identifiable neurons and neuron classes to lamprey vertebrate neurobiology. *Prog Neurobiol* 63: 441–466, 2001.

Bui TV, Cushing S, Dewey D, Fyffe RE, and Rose PK. Comparison of the morphological and electrotonic properties of Renshaw cells, Ia inhibitory interneurons, and motoneurons in the cat. *J Neurophysiol* 90: 2900–2918, 2003.

Butt SJ, Lundfald L, and Kiehn O. EphA4 defines a class of excitatory locomotor-related interneurons. *Proc Natl Acad Sci USA* 102: 14098–14103, 2005.

Caspary T and Anderson KV. Patterning cell types in the dorsal spinal cord: what the mouse mutants say. *Nat Rev Neurosci* 4: 289–297, 2003.

Cheng J, Jovanovic K, Aoyagi Y, Bennett DJ, Han Y, and Stein RB. Differential distribution of interneurons in the neural networks that control walking in the mudpuppy (Necturus maculatus) spinal cord. *Exp Brain Res* 145: 190–198, 2002.

Clarac F, Pearlstein E, Pflieger JF, and Vinay L. The in vitro neonatal rat spinal cord preparation: a new insight into mammalian locomotor mechanisms. *J Comp Physiol [A]* 190: 343–357, 2004.

Drew T and Doucet S. Application of circular statistics to the study of neuronal discharge during locomotion. *J Neurosci Methods* 38: 171–181, 1991.

Drew T, Prentice S, and Schepens B. Cortical and brainstem control of locomotion. *Prog Brain Res* 143: 251–261, 2004.

Edgley SA. Organisation of inputs to spinal interneurone populations. *J Physiol* 533: 51–56, 2001.

Fernandez A, Radmilovich M, Russo RE, Hounsgaard J, and Trujillo-Cenoz O. Monosynaptic connections between primary afferents and giant neurons in the turtle spinal dorsal horn. *Exp Brain Res* 108: 347–356, 1996.

Fetcho JR. The spinal motor system in early vertebrates and some of its evolutionary changes. *Brain Behav Evol* 40: 82–97, 1992.

Fyffe RE. Evidence for separate morphological classes of Renshaw cells in the cat's spinal cord. *Brain Res* 536: 301–304, 1990.

Gorman RB, McDonagh JC, Hornby TG, Reinking RM, and Stuart DG. Measurement and nature of firing rate adaptation in turtle spinal neurons. *J Comp Physiol [A]* 191: 583–603, 2005.

Grillner S. The motor infrastructure: from ion channels to neuronal networks. *Nat Rev Neurosci* 4: 573–586, 2003.

Grillner S and Dubuc R. Control of locomotion in vertebrates: spinal and supraspinal mechanisms. In: *Functional Recovery in Neurological Disease*, edited by Waxman SG. New York: Raven Press, 1988, p. 425–453.

Hale ME, Ritter DA, and Fetcho JR. A confocal study of spinal interneurons in living larval zebrafish. *J Comp Neurol* 437: 1–16, 2001.

Higashijima S, Masino MA, Mandel G, and Fetcho JR. Engrailed-1 expression marks a primitive class of inhibitory spinal interneuron. *J Neurosci* 24: 5827–5839, 2004.

Hinckley CA, Hartley R, Wu L, Todd A, and Ziskind-Conhaim L. Locomotor-like rhythms in a genetically distinct cluster of interneurons in the mammalian spinal cord. *J Neurophysiol* 93: 1439–1449, 2005.

Hounsgaard J and Kjaerulff O. Ca^{2+}-mediated plateau potentials in a subpopulation of interneurons in the ventral horn of the turtle spinal cord. *Eur J Neurosci* 4: 183–188, 1992.

Hounsgaard J and Nicholson C. The isolated turtle brain and the physiology of neuronal circuits. In: *Preparations of Vertebrate Central Nervous System In Vitro*, edited by Jahnsen H. New York: John Wiley, 1990, p. 155–181.

Jankowska E. Interneuronal relay in spinal pathways from proprioceptors. *Prog Neurobiol* 38: 335–378, 1992.

Kiehn O and Butt SJ. Physiological, anatomical and genetic identification of CPG neurons in the developing mammalian spinal cord. *Prog Neurobiol* 70: 347–361, 2003.

Kusuma A, ten Donkelaar HJ, and Nieuwenhuys R. Intrinsic organization of the spinal cord. In: *Biology of the Reptilia,* edited by Gans C, Northcutt RG, and Ulinski P. New York: Academic Press, 1979, vol. 10, p. 59–109.

Lanuza GM, Gosgnach S, Pierani A, Jessell TM, and Goulding M. Genetic identification of spinal interneurons that coordinate left-right locomotor activity necessary for walking movements. *Neuron* 42: 375–386, 2004.

Lewis KE. How do genes regulate simple behaviours? Understanding how different neurons in the vertebrate spinal cord are genetically specified. *Philos Trans R Soc Biol Sci* 361: 45–66, 2006.

Li WC, Higashijima S, Parry DM, Roberts A, and Soffe SR. Primitive roles for inhibitory interneurons in developing frog spinal cord. *J Neurosci* 24: 5840–5848, 2004.

Li WC, Perrins R, Soffe SR, Yoshida M, Walford A, and Roberts A. Defining classes of spinal interneuron and their axonal projections in hatchling Xenopus laevis tadpoles. *J Comp Neurol* 441: 248–265, 2001.

Lutz PL, Nilsson GE, and Prentice HM. *The Brain Without Oxygen.* Dordrecht, The Netherlands: Kluwer Academic Publishers, 2003.

Marder E and Calabrese RL. Principles of rhythmic motor pattern generation. *Physiol Rev* 76: 687–717, 1996.

Mardia KV. *Statistics of Directional Data.* London: Academic Press, 1972.

Matsuyama K, Nakajima K, Mori F, Aoki M, and Mori S. Lumbar commissural interneurons with reticulospinal inputs in the cat: morphology and discharge patterns during fictive locomotion. *J Comp Neurol* 474: 546–561, 2004.

McDonagh JC, Gorman RB, Gilliam EE, Hornby TG, Reinking RM, and Stuart DG. Properties of spinal motoneurons and interneurons in the adult turtle: provisional classification by cluster analysis. *J Comp Neurol* 400: 544–570, 1998.

McDonagh JC, Hornby TG, Reinking RM, and Stuart DG. Associations between the morphology and physiology of ventral-horn neurons in the adult turtle. *J Comp Neurol* 454: 177–191, 2002.

Nieuwenhuys R. Comparative anatomy of the spinal cord. *Prog Brain Res* 11: 1–55, 1964.

Nissen UV, Mochida H, and Glover JC. Development of projection-specific interneurons and projection neurons in the embryonic mouse and rat spinal cord. *J Comp Neurol* 483: 30–47, 2005.

O'Donovan MJ, Wenner P, Chub N, Tabak J, and Rinzel J. Mechanisms of spontaneous activity in the developing spinal cord and their relevance to locomotion. *Ann NY Acad Sci* 860: 130–141, 1998.

Oppenheim RW, Shneiderman A, Shimizu I, and Yaginuma H. Onset and development of intersegmental projections in the chick embryo spinal cord. *J Comp Neurol* 275: 159–180, 1988.

Orlovsky GN, Deliagina TG, and Grillner S. *Neuronal Control of Locomotion: From Mollusc to Man.* Oxford, UK: Oxford, 1999.

Rastad J, Gad P, Jankowska E, McCrea D, and Westman J. Light microscopical study of dendrites and perikarya of interneurones mediating la reciprocal inhibition of cat lumbar alpha-motoneurones. *Anat Embryol* 181: 381–388, 1990.

Roberts A. Early functional organization of spinal neurons in developing lower vertebrates. *Brain Res Bull* 53: 585–593, 2000.

Robertson GA, Mortin LI, Keifer J, and Stein PSG. Three forms of the scratch reflex in the spinal turtle: central generation of motor patterns. *J Neurophysiol* 53: 1517–1534, 1985.

Robertson GA and Stein PSG. Synaptic control of hindlimb motoneurones during three forms of the fictive scratch reflex in the turtle. *J Physiol* 404: 101–128, 1988.

Ruigrok TJH and Crowe A. The organization of motoneurons in the turtle lumbar spinal cord. *J Comp Neurol* 228: 24–37, 1984.

Ruigrok TJH, Crowe A, and ten Donkelaar HJ. Morphology of lumbar motoneurons innervating hindlimb muscles in the turtle *Pseudemys scripta elegans*: an intracellular horseradish peroxidase study. *J Comp Neurol* 230: 413–425, 1984.

Russo RE and Hounsgaard J. Burst-generating neurones in the dorsal horn in an in vitro preparation of the turtle spinal cord. *J Physiol* 493: 55–66, 1996a.

Russo RE and Hounsgaard J. Plateau-generating neurones in the dorsal horn in an in vitro preparation of the turtle spinal cord. *J Physiol* 493: 39–54, 1996b.

Scheibel ME and Scheibel AB. A structural analysis of spinal interneurons and Renshaw cells. In: *The Interneuron*, edited by Brazier MAB. Berkeley, CA: University of California, 1969, p. 159–208.

Sharma K and Peng CY. Spinal motor circuits: merging development and function. *Neuron* 29: 321–324, 2001.

Silos-Santiago I and Snider WD. Development of commissural neurons in the embryonic rat spinal cord. *J Comp Neurol* 325: 514–526, 1992.

Silos-Santiago I and Snider WD. Development of interneurons with ipsilateral projections in embryonic rat spinal cord. *J Comp Neurol* 342: 221–231, 1994.

Stauffer EK, Stuart DG, McDonagh JC, Hornby TG, and Reinking RM. Afterhyperpolarization-firing rate relation of turtle spinal neurons. *J Comp Physiol [A]* 191: 135–146, 2005.

Stein PSG. Neuronal control of turtle hindlimb motor rhythms. *J Comp Physiol [A] Neuroethol Sens Neural Behav Physiol* 191: 213–229, 2005.

Wilson JM, Hartley R, Maxwell DJ, Todd AJ, Lieberam I, Kaltschmidt JA, Yoshida Y, Jessell TM, and Brownstone RM. Conditional rhythmicity of ventral spinal interneurons defined by expression of the Hb9 homeodomain protein. *J Neurosci* 25: 5710–5719, 2005.

Yaginuma H, Shiga T, and Oppenheim RW. Early developmental patterns and mechanisms of axonal guidance of spinal interneurons in the chick embryo spinal cord. *Prog Neurobiol* 44: 249–278, 1994.